Available online at www.sciencedirect.com
SCIENCE DIRECT®
ELSEVIER
Earth and Planetary Science Letters 216 (2003) 645–661
EPSL
www.elsevier.com/locate/epsl

Seismic evidence for deep low-velocity anomalies in the transition zone beneath West Antarctica

Anne Sieminski *, Eric Debayle, Jean-Jacques Lévêque

IPGS – Ecole et Observatoire des Sciences de la Terre, CNRS and Université Louis Pasteur, 5 rue René Descartes, 67084 Strasbourg, France

Received 13 June 2003; received in revised form 10 September 2003; accepted 15 September 2003

Abstract

We present a three-dimensional (3D) SV-wave velocity model of the upper mantle beneath the Antarctic plate constrained by fundamental and higher mode Rayleigh waves recorded at regional distances. The good agreement between our results and previous surface wave studies in the uppermost 200 km of the mantle confirms that despite strong differences in data processing, modern surface wave tomographic techniques allow to produce consistent velocity models, even at regional scale. At greater depths the higher mode information present in our data set allows us to improve the resolution compared to previous regional surface wave studies in Antarctica that were all restricted to the analysis of the fundamental mode. This paper is therefore mostly devoted to the discussion of the deeper part of the model. Our seismic model displays broad domains of anomalously low seismic velocities in the asthenosphere. Moreover, we show that some of these broad, low-velocity regions can be more deeply rooted. The most remarkable new features of our model are vertical low-velocity structures extending from the asthenosphere down to the transition zone beneath the volcanic region of Marie Byrd Land, West Antarctica and a portion of the Pacific–Antarctic Ridge close to the Balleny Islands hotspot. A deep low-velocity anomaly may also exist beneath the Ross Sea hotspot. These vertical structures cannot be explained by vertical smearing of shallow seismic anomalies and synthetic tests show that they are compatible with a structure narrower than 200 km which would have been horizontally smoothed by the tomographic inversion. These deep low-velocity anomalies may favor the existence of several distinct mantle plumes, instead of a large single one, as the origin of volcanism in and around West Antarctica. These hypothetical deep plumes could feed large regions of low seismic velocities in the asthenosphere.

Keywords: upper mantle; Antarctica; plume; surface waves; tomography

1. Introduction

There seems to be a consensus on the general outline of the structure and evolution of Antarctica even though this region still raises many open questions. The Antarctic continent is divided into two geologically different entities. East Antarctica (Fig. 1a) is a stable Precambrian shield and was a segment of the core of the Gondwanaland supercontinent that was assembled during the Neoproterozoic. West Antarctica consists of several arc

* Corresponding author.
E-mail address: anne.sieminski@eost.u-strasbg.fr (A. Sieminski).

0012-821X/03/$ – see front matter © 2003 Elsevier B.V. All rights reserved.
doi:10.1016/S0012-821X(03)00518-1

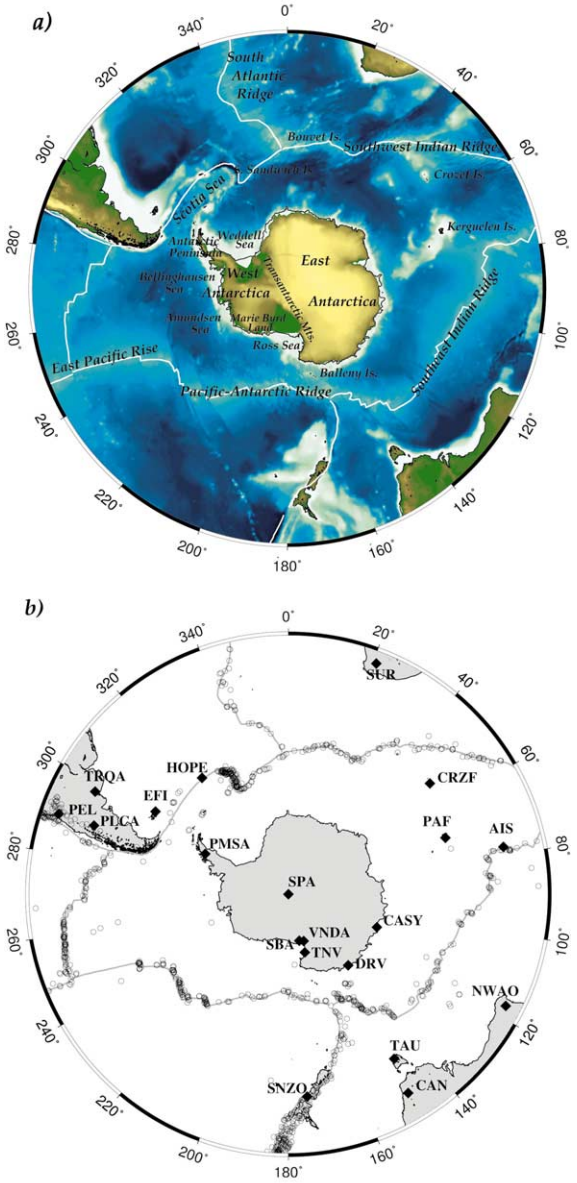

Fig. 1. Map of Antarctica and surrounding oceans. (a) Location of some of the regions concerned in text and the main plate boundaries (white lines) (b) Stations (diamonds) and events (open circles) considered in the study.

and forearc elements inherited from the complex circum-Pacific convergent margin since the Cambrian. These elements have been accreted together with displaced fragments of the craton on the western margin of the East Antarctic shield during the Paleozoic [1]. The crust has an average thickness of about 40 km beneath East Antarctica while it is thinner (~25 km in average) in West Antarctica [2]. West Antarctica is separated from the East Antarctic Craton by the Transantarctic Mountains, a large mountain range extending from the Ross Sea to the Weddell Sea (Fig. 1a). The West Antarctic rift system follows the western flank of the Transantarctic Mountains to the basis of the Antarctic Peninsula. It results of late Mesozoic and Cenozoic extension between East and West Antarctica and is one of the largest active continental rift systems [3]. Volcanism is present in West Antarctica but its origin is still debated. Although the volcanic rocks are geographically associated to the rift, they have erupted from 30 Ma with the major activity at Neogene time to present [4] while most extension in West Antarctica occurred with the rifting of New Zealand, in the late Cretaceous [5]. Evidences of a more recent Cenozoic motion between East and West Antarctica have recently been presented [3] but the connection with the West Antarctic Rift is still discussed (e.g. [6]). If the volcanism is not entirely due to the rifting it could involve a mantle plume beneath the region [5,7–9]. This hypothesis is based on the amount of volcanic rocks together with their geochemical characteristics and tectonic doming. Middle Jurassic basalts have also been found along the Transantarctic Mountains. They form the Ferrar traps issued from the breakup of the Gondwanaland [10].

Seismic tomography of the upper mantle beneath the region could provide valuable information to discuss the cause of volcanism. Global studies with a lateral resolution of about 1000 km imaged the large-scale features of the lithosphere and upper mantle in the region (e.g. [11,12]). The East Antarctic Craton is associated to high-velocity anomalies while West Antarctica is underlain by low velocities. Further knowledge of the regional dynamics requires seismic studies at a more detailed scale. Due to the relatively small number of seismic stations at high southern latitudes, surface waves are presently the most relevant tool to probe the upper mantle in these regions. Few surface wave studies have been car-

ried out in the Antarctic region so far [2,6,13–15]. With an improved lateral resolution reaching few hundred kilometers, these studies showed the complexity of the craton by providing more details on its structure, its depth extent (~200–225 km) and its boundary with West Antarctica. They also allowed to image low-velocity anomalies in the asthenosphere beneath most of the regional hotspots. However, these regional studies were all restricted to the analysis of the fundamental mode of surface waves only and their poor resolution at depth greater than 200 km did not allow to confirm nor rule out the mantle plume hypothesis in West Antarctica.

In this paper we present a three-dimensional (3D), SV-wave velocity model of the upper mantle beneath the Antarctic plate. The model has been obtained from the waveform inversion of 3350 Rayleigh wave seismograms. Overtones as well as fundamental mode data have been taken into account in the processing. This allows us to gain some resolution at depth larger than 200 km, which is an improvement compared to previous studies. The model reveals a heterogeneous upper mantle at 200–250 km depth with broad, low-velocity anomalies in the asthenosphere. Some of these anomalies are deeply rooted. In the vicinity of West Antarctica and the Balleny Islands hotspot, we observe remarkable vertical low-velocity structures extending from the asthenosphere to the transition zone, suggesting the existence of at least two distinct mantle plumes that could be related to the volcanism observed in and around West Antarctica.

2. Data

The region under study is situated south of 30°S and encompasses Antarctica and the surrounding oceans (Fig. 1a). We analyzed the Rayleigh wave portion of long-period vertical seismograms recorded at regional distances on 20 permanent IRIS, GEOSCOPE, GTSN and MEDNET stations in the region (Fig. 1b). The selected events occurred from 1989 to February 2002 mainly on the ridges circling Antarctica and at the subduction trenches of Chile, New Zealand and South Sandwich Islands (Fig. 1b). The analysis is conducted with the automated version [16] of Cara and Lévêque's [17] waveform inversion approach (see Section 3 for details). From an initial database of 14 100 Rayleigh wave seismograms analyzed, 3350 passed successfully the stringent tests of the automated procedure and were included in the tomographic inversion. Our waveform analysis allows us to model the fundamental mode and up to four overtones in the period range 50–160 s. A large number of seismograms correspond to intermediate size earthquakes recorded at relatively short epicentral distances (70% of the paths are shorter than 6500 km) so that periods larger than 100 s are considered for only 44% of the paths. The use of the overtones in the 50–100 s period range is however largely sufficient to achieve a good resolution in the whole upper mantle (e.g. [12,18]). At least one overtone was considered for 1275 paths while the fundamental mode was taken into account for all the 3350 paths. Fig. 2a shows that the central part of the region under study is densely covered. The ray density is lower on the edges, especially in the South Pacific Ocean where there is no permanent station for latitudes south of 30°S. The path coverage for the data for which at least one overtone is modelled is less dense (Fig. 2b) but it is still homogeneous.

3. Tomographic procedure

The building of our tomographic model is a two-step process that has been previously applied to study the upper mantle beneath the Indian Ocean [19], Australia [16,20], northeastern Africa [18], Asia [21], and the North Atlantic Ocean [22]. We refer to these papers for a detailed presentation of the two-step approach and focus here on the choices specific to this study.

In the first step, we use the automated version [16] of Cara and Lévêque's [17] waveform inversion technique to model each individual Rayleigh waveform in terms of a one-dimensional (1D) SV-wave velocity model representing the average mantle structure along the path. A detailed discussion of the application of Cara and Lévêque's

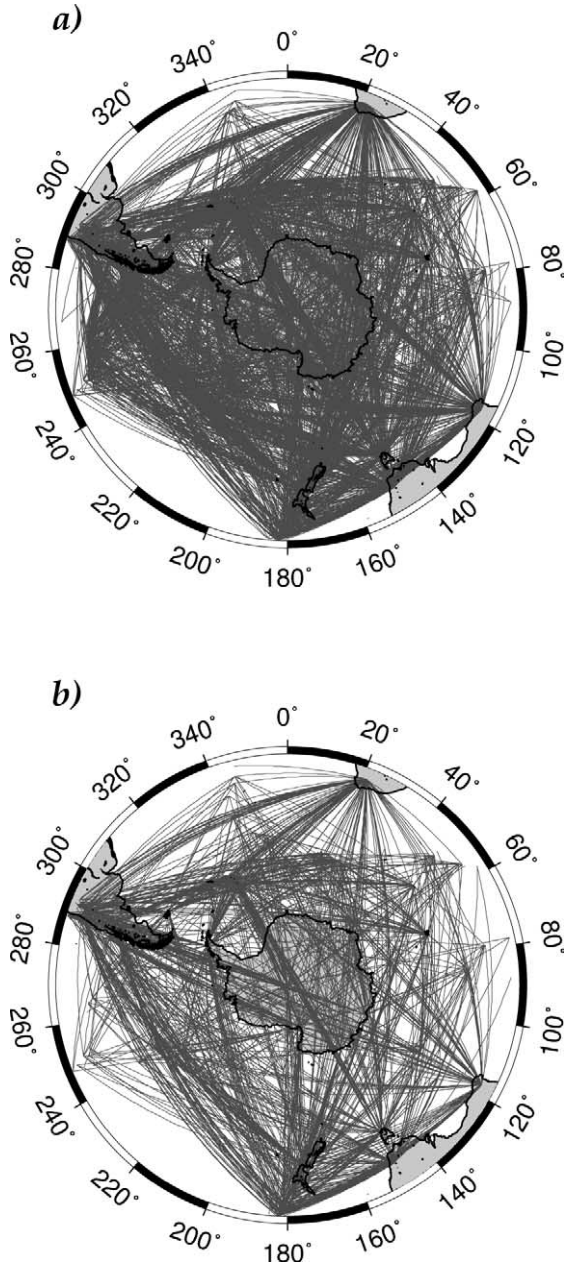

Fig. 2. Path coverage related to (a) the 3350 paths for which the fundamental mode has been modelled, (b) the 1275 paths for which at least one overtone has been modelled.

[17] technique to several multimode Rayleigh wave seismograms can be found in [23]. We invert for the upper mantle structure only and use a smoothed version of PREM [24] as a starting upper mantle model (Fig. 3). To avoid bias of crustal origin in the inverted mantle model, the crust is specifically adapted to each path by averaging the crustal part of the a priori 3SMAC model [25] along the source-receiver great circle path.

In a second step, we combine the 1D path average models into a linear tomographic inversion to retrieve the local SV-wave velocity structure. The inversion is performed using the continuous regionalization algorithm of Montagner [26] assuming propagation along the great circle. The lateral smoothness of the model is constrained by correlating neighboring points using a Gaussian a priori covariance function which is characterized by two tuning parameters: the width of the a priori Gaussian, defined through a horizontal correlation length L_{corr} which controls the degree of horizontal smoothing in the inverted model and the amplitude of the a priori Gaussian, defined at each geographical point r by an a priori standard deviation $\sigma(r)$ which in some way controls the amplitude of the perturbations in the inverted model. After several trials, we chose a value of 400 km for L_{corr}, meaning that a correlation coefficient of 0.6 is a priori imposed between two points distant of 400 km. Considering that 400

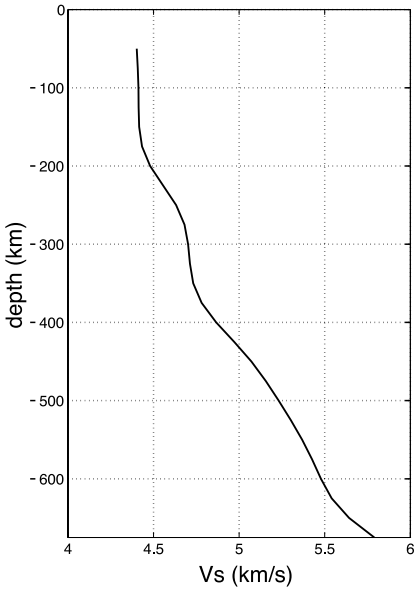

Fig. 3. Smoothed version of PREM [24] used in the study.

km is about the wavelength of a Rayleigh wave at 100 s period, our choice is equivalent to assume for a majority of the paths a significant a priori correlation between two points distant from a wavelength. The a priori standard deviation $\sigma(r)$ was taken equal to 0.05 km/s according to the commonly observed SV-wave velocity variations (see e.g. [19] or [27]).

Providing that the azimuthal distribution of paths is sufficient, Montagner's [26] approach can be used to retrieve the SV-wave azimuthal anisotropy in addition to the SV-wave heterogeneities. Lévêque et al. [28] describe in detail the procedure to follow and conclude that even in fully anisotropic structure, the velocity of horizontally propagating long-period SV-waves, in a

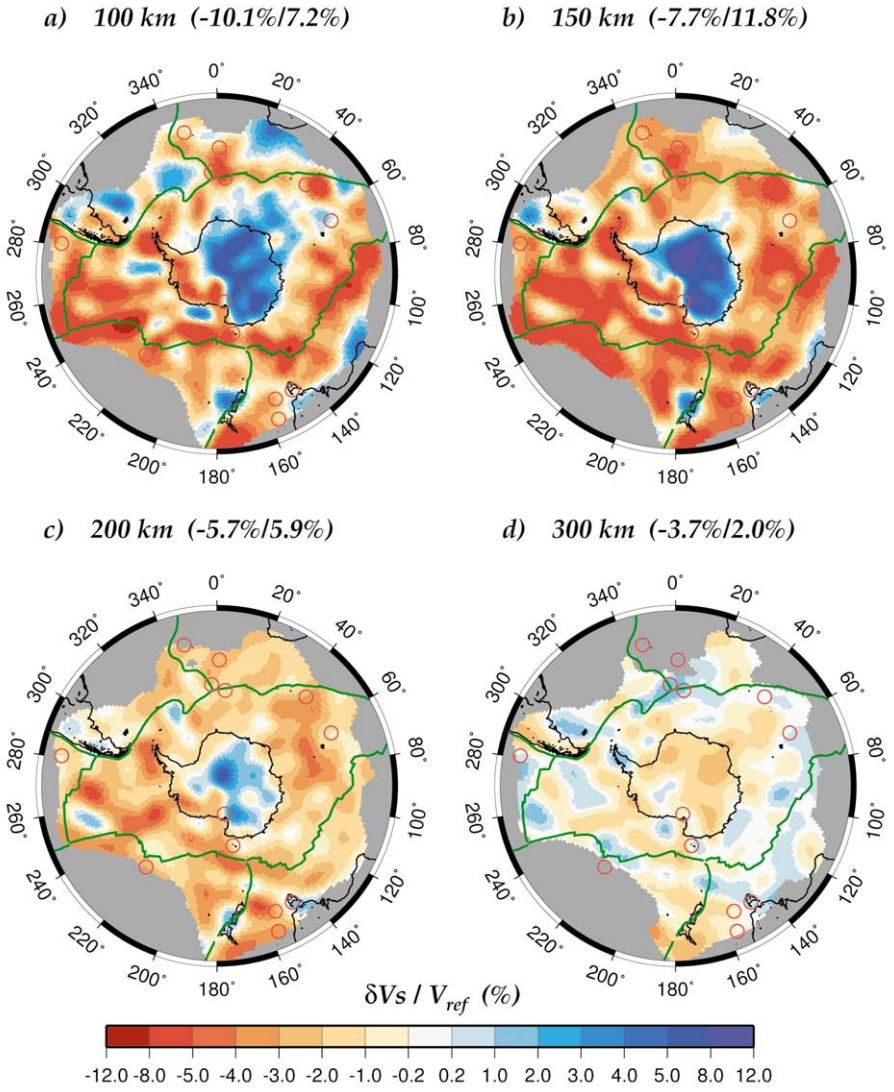

Fig. 4. Maps of the SV velocity variations relative to our smoothed version of PREM (Fig. 3) at (a) 100 km depth, (b) 150 km depth, (c) 200 km depth and (d) 300 km depth. The range of velocity variations is given for each map. Regions where the resolution is poor (error ≥ 0.04 km/s) are in gray (Fig. 5). Green lines are the main plate boundaries and red open circles represent the hotspots of Duncan and Richards's [36] distribution.

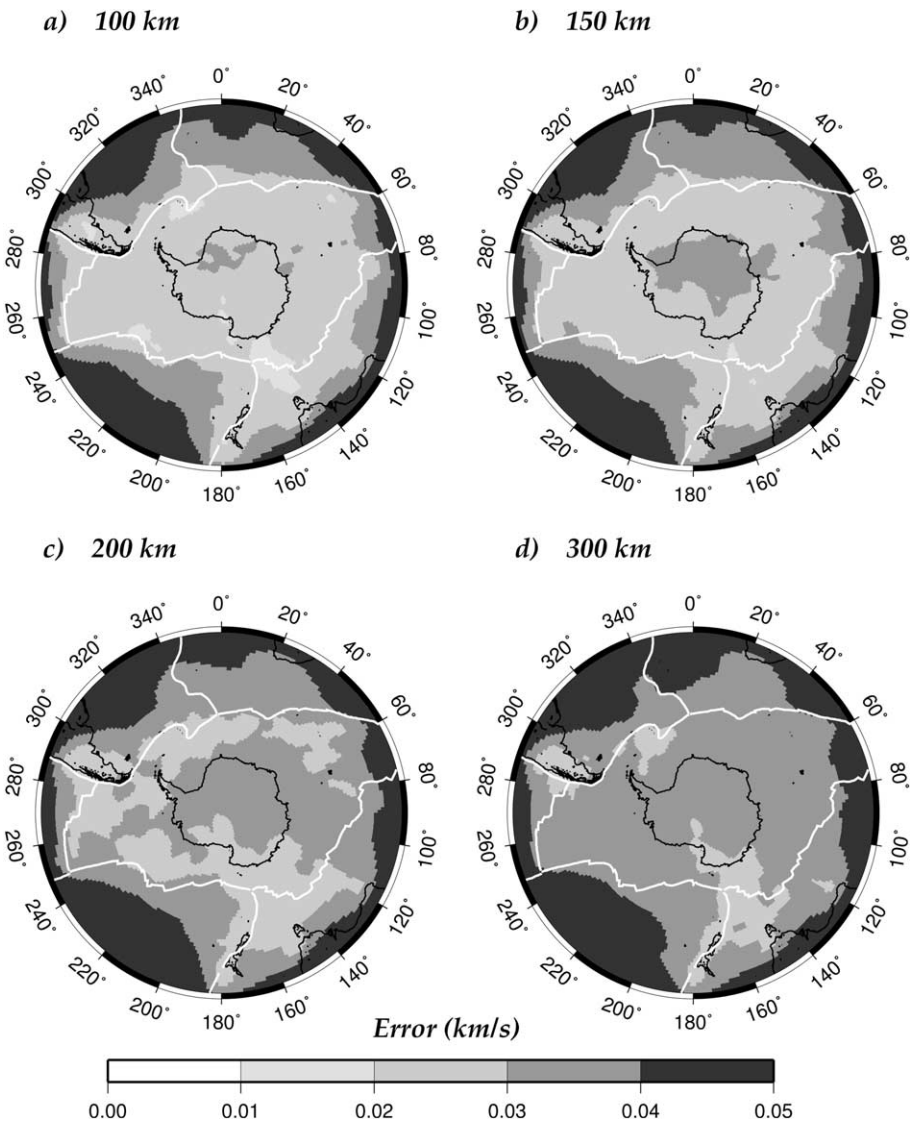

Fig. 5. Maps of the a posteriori error at (a) 100 km depth, (b) 150 km depth, (c) 200 km depth and (d) 300 km depth.

depth range controlled by the period and the rank of the mode, is the most influential factor in the first-order variation of surface wave phase velocities. In this study, the ray density and the azimuthal distribution of paths allow us to invert for both the SV-wave velocity and azimuthal anisotropy and we have undertaken different style of inversions, including azimuthal anisotropy or not.

4. Tomographic maps

The SV-wave velocity model presented here has been obtained from an inversion including azimuthal anisotropy with $L_{\mathrm{corr}} = 400$ km, $\sigma_{\mathrm{i}}(r) = 0.05$ km/s for the isotropic parameter and $\sigma_{\mathrm{a}}(r) = 0.003$ km/s for the anisotropic parameters. This model gives the best compromise between data fitting and physically reasonable values for the

inverted model. Trying different values of L_{corr} and $\sigma_a(r)$ (200 km $\leq L_{corr} \leq$ 1000 km, $0 \leq \sigma_a(r) \leq 0.005$ km/s) leaves the results very stable with respect to the conclusions we can draw.

For example, an inversion that does not include azimuthal anisotropy produces slightly larger amplitudes for the SV-wave heterogeneities but does not change the pattern of seismic anomalies so that our conclusions are unchanged whether anisotropy is included in the inversion or not. As expected, with $L_{corr} \geq 400$ km, the inverted models are smoother but the pattern of SV-wave heterogeneities is otherwise essentially unchanged.

Our preferred model concentrates azimuthal anisotropy in the uppermost 200 km of the mantle with a maximum value of 5.2% of peak-to-peak azimuthal anisotropy at 100 km depth, decreasing to 1.5% at 200 km and to values smaller than 1% at greater depths. These results are consistent with the previous observations of upper mantle anisotropy beneath Antarctica by Roult et al. [13] for azimuthal anisotropy and Ritzwoller et al. [6] for radial anisotropy. Both studies suggest that a few percent anisotropy exists and is confined to the shallower 200–250 km of the mantle. We therefore do not discuss anisotropy results in this paper but rather focus on the deep SV-wave structure, especially at depth greater than 200 km where seismic anisotropy is no more significant.

Velocity maps are shown in Fig. 4 for selected depths from 100 to 300 km. Velocity variations are calculated relative to our smoothed version of PREM (Fig. 3). A way to assess the quality of the inverted model is to look at the diagonal terms of the a posteriori covariance matrix. The regions where this a posteriori error is close to the a priori error (we fix the threshold at 0.04 km/s, 80% of the 0.05 km/s a priori error) can be regarded as regions of poor resolution. They are displayed in gray on the maps in Fig. 4. A general trend exists for the error to increase with depth (Fig. 5). This is related to a reduction of information on the model at depth due to a limited number of paths for which overtones have been analyzed. However the central zone displays an a posteriori error lower than the 0.04 km/s threshold down to 675 km depth. The 95% confidence level in the results (two standard deviations or twice the a posteriori error) thus corresponds here to a velocity contrast of $\sim$1.6% for the deeper part of the model. However it is very common in the literature to consider that velocity perturbations greater than once the a posteriori error (the 68% confidence level in the results) are meaningful. Using this weaker criterion anomalies of at least 1% in the central zone could be interpreted.

Our observations for the uppermost 200 km of the mantle can be summarized as follows. In this shallowest part of the mantle (Fig. 4a and b) we observe the largest velocity variations and a good correlation with surface tectonics. In this depth range our results are also in good agreement with previous global and regional studies. For example, we retrieve the sharp transition between the high-velocity pattern of the East Antarctic Craton and the low velocities beneath West Antarctica previously observed at global (e.g. [12]) and regional [6,13,15] scales, although the bound-

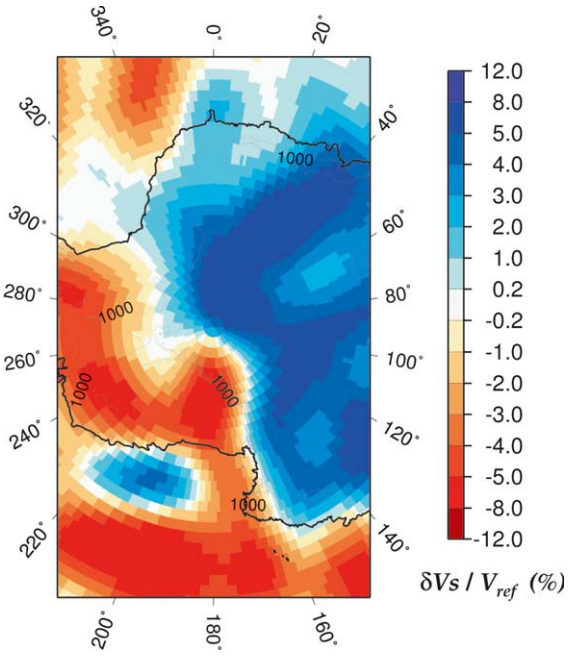

Fig. 6. SV-wave velocity variations at 100 km depth beneath the Transantarctic Mountains. The topographic contours at 1000 and 2000 m are plotted. They mark the western flank of the Transantarctic Mountains. Note the rather good correlation between the western flank of the Transantarctic Mountains and the transition between high and low velocities.

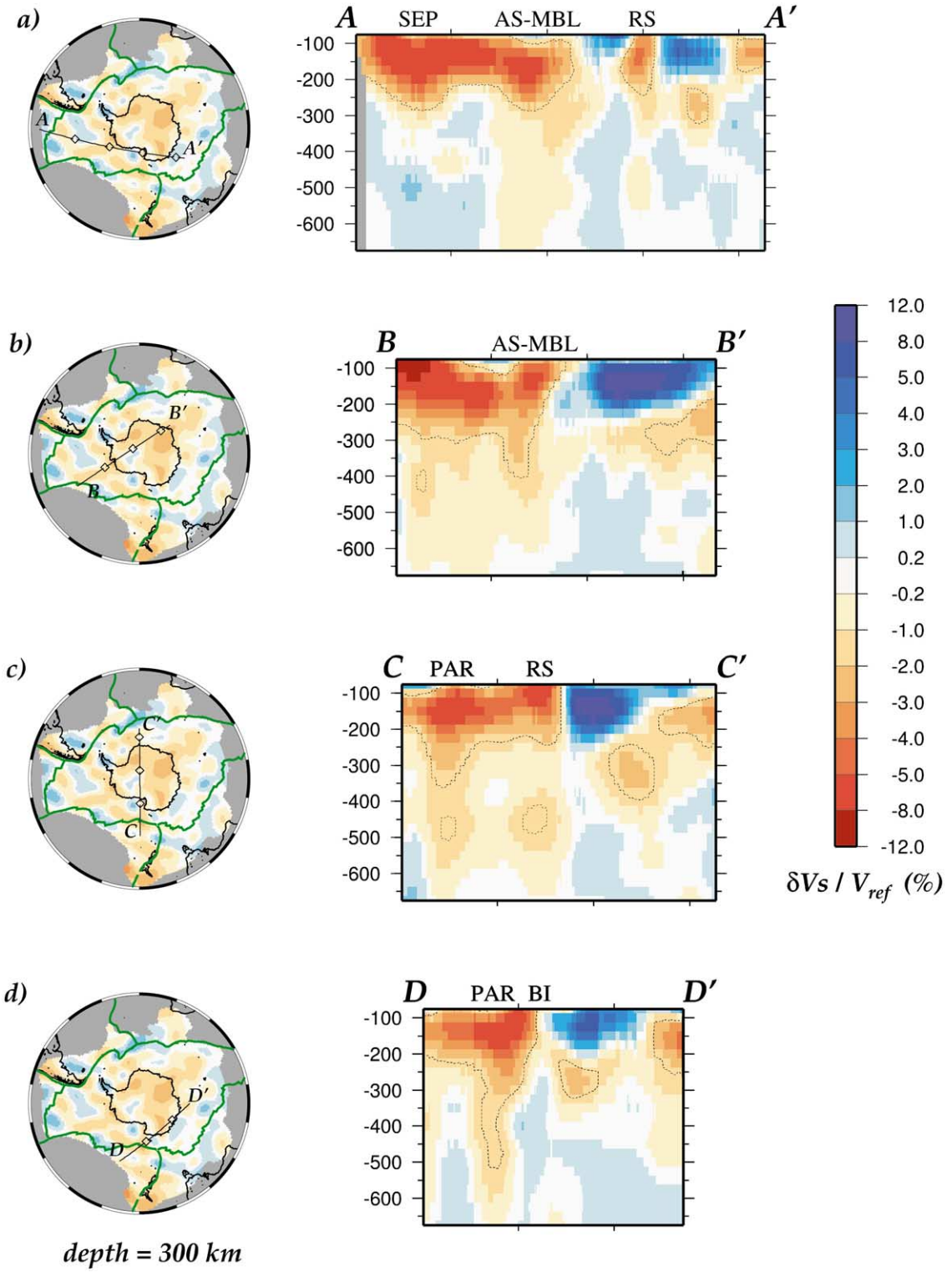
a)
A
A′
A
SEP
AS-MBL
RS
A′
-100
-200
-300
-400
-500
-600
b)
B′
B
B
AS-MBL
B′
c)
C′
C
C
PAR
RS
C′
d)
D′
D
D
PAR_BI
D′
12.0
8.0
5.0
4.0
3.0
2.0
1.0
0.2
-0.2
-1.0
-2.0
-3.0
-4.0
-5.0
-8.0
-12.0
δVs / V_ref (%)
depth = 300 km

Fig. 7.

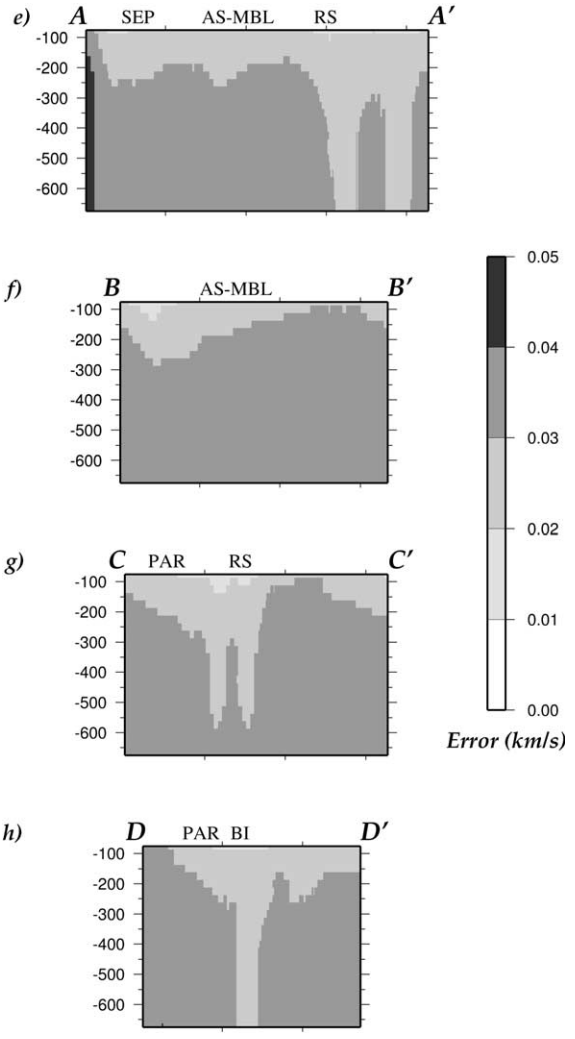

Fig. 7 (*Continued*). (a), (b), (c) and (d) Vertical cross-sections from 75 to 675 km depth along the profiles plotted on the maps presented on the left of the cross-sections. The velocity variations are calculated relatively to a smoothed version of PREM (Fig. 3). The contour line displays the −1.6% velocity perturbation which roughly corresponds to twice the a posteriori error (95% confidence level in the results) for depths below 300 km. Empty diamonds are plotted at 20° intervals on the paths and correspond to the tickmarks on the cross-sections. Labels above the cross-sections refer to anomalies and regions discussed in text (SEP, Southeast Pacific; AS–MBL, Amundsen Sea–Marie Byrd Land; RS, Ross Sea; PAR, Pacific–Antarctic Ridge; and BI, Balleny Islands). (e), (f), (g) and (h) A posteriori error cross-sections corresponding to the cross-sections of (a), (b), (c) and (d). Note that the a posteriori error in all four cross-sections is smaller than 0.04 km/s down to 675 km depth (except on the left edge of cross-section AA′).

ary is not as straight as it was found in [15]. We find in our model a good correlation between the western flank of the Transantarctic Mountains and the transition from the East Antarctica high velocities to the West Antarctica low velocities (Fig. 6). We also observe a moderately thick high-velocity anomaly beneath the East Antarctic Craton which locally reaches 225 km depth (Fig. 4c and cross-sections in Fig. 7). This agrees with previous results for Antarctica [6,13,15] and with recent surface wave observations beneath other cratons [20,21,29].

In oceanic areas, the low-velocity signature of the mid-oceanic ridges surrounding Antarctica is rather shallow and vanishes at 150 km depth. The amplitude of the seismic anomaly is correlated with spreading rates, the strongest low-velocity anomalies being associated with the fastest ridges (the East Pacific Rise, the South East Indian Ridge, see Fig. 4a). An exception is the Australian–Antarctic Discordance (AAD), a peculiar region of the South East Indian Ridge lying between 120°E and 127°E. In our model, this area is associated with a structure relatively fast compared to the neighboring portions of the ridge. This agrees with the results of Forsyth et al. [30] and with the more recent works of Debayle and Lévêque [19] and Ritzwoller et al. [6]. In addition to the relatively fast-velocity pattern, the AAD region has been associated with a thin crust, a deep bathymetry, a rough topography, a gravity anomaly and a geoid low [30]. All these observations can be explained by a colder and more viscous region in the mantle beneath the AAD [30,31]. The positive heterogeneities in the Amundsen-Bellinghausen Sea and in the South Indian Ocean at 100 km depth (Fig. 4a) suggest the presence of an old, thick oceanic lithosphere in regions where the age of the oceanic sea floor is poorly known [32]. In the vicinity of most regional hotspots (Crozet, Balleny, Erebus, Tasmanid and the Atlantic hotspots of Bouvet, Shona and Discovery), we observe negative anomalies in the depth range 150–200 km, with the exception of the proposed location of the Kerguelen hotspot. However, all these hotspots are situated in the oceanic part of the model which mostly displays low velocities in this depth range. The coincidence

between hotspot and negative anomaly is thus not significant for these depths.

At regional scale, Ritzwoller et al. [6] achieved the most comprehensive ray coverage of Antarctica with several thousands of fundamental mode surface wave measurements, compared to the few hundred seismograms used by Roult et al. [13] or Danesi and Morelli [15]. Ritzwoller et al. [6] analyzed a data set of Rayleigh and Love, phase and group velocity measurements while we directly invert Rayleigh waveforms to retrieve path average SV-wave velocity models. Phase and group velocities are theoretically redundant data but Shapiro and Ritzwoller [33] showed that the simultaneous inversion of phase and group velocities reduces significantly uncertainties at all depths. Analyzing the waveforms as we do (i.e. fitting envelope and phase) is very similar to a simultaneous inversion of both group and phase velocities and presents the advantage to allow simultaneous inversion of fundamental and higher mode data. Ritzwoller et al. [6] performed their analysis of the fundamental mode in the period range 18–175 s while we use fundamental and higher modes between 50 s and 160 s. A 175 s fundamental mode Rayleigh wave reaches its maximum sensitivity between 250 and 300 km depth. Below this depth their model should have a decreasing resolution, whereas the higher modes in the period range we use are still sensitive to the structure below 600 km depth. Considering Love waves in addition to Rayleigh waves gives access to the radial anisotropy and should provide more constraint as Love waves have a different sensitivity to the structure in depth. On the other hand, Love wave records are usually very noisy and introducing these data could impair the accuracy of the results. In this study, as we are mainly interested in the velocity structure, we choose to analyze only high-quality Rayleigh wave records. Our sampling of the uppermost 200 km of the mantle, largely constrained by the fundamental mode of Rayleigh waves at intermediate periods is probably very similar to the one achieved by Ritzwoller et al. [6]. They present shear wave velocity maps down to 250 km and several vertical cross-sections in the shear velocity model [6]. Even though they display SV-wave and SH-wave velocity variations relatively to a different reference model, AK135 [34], the pattern of the velocity anomalies can be directly compared with our results. Our vertical profile BB′ (Fig. 7b) has been chosen very close to the one presented in their paper [6] (vertical section CC′ in plate 5). The agreement in the uppermost 200 km between both models is striking, especially for the uppermost part of both vertical sections.

The main features of our model at 200 km depth (Fig. 4c) are broad, low-velocity anomalies in the oceanic regions reaching 3%. On the vertical cross-sections of Fig. 7 several of them look like downward extensions of an otherwise relatively thin low-velocity layer (~175 km thick) that we interpret as the asthenosphere. Moreover, more remarkable deep anomalies are also present in our model. For example, profile AA′ crosses two of the large, low-velocity anomalies located in the Southeast Pacific Ocean (labelled SEP in Fig. 7a) and in the Amundsen Sea–Marie Byrd Land region (labelled AS–MBL). The latter extends down to 450 km depth beneath the coast of Marie Byrd Land where its amplitude remains greater than 1% (see Fig. 1a and cross-section BB′ in Fig. 7b), while the low-velocity anomaly in the Southeast Pacific Ocean (SEP) vanishes at shallower depths, between 250 and 300 km depth, like the broad, low-velocity anomalies beneath the Antarctic Peninsula and south of Crozet and Kerguelen Islands (Fig. 4c). The low-velocity anomaly located beneath the Ross Sea region (RS) presents an amplitude greater than 1% down to 300 km depth in Fig. 7a. In cross-section CC′ (Fig. 7c), the same anomaly has an amplitude greater than 1% from the surface down to 550 km, except between 250 and 380 km where it slightly passes below 1%. On cross-sections CC′ and DD′, another continuous low-velocity vertical structure with an amplitude greater than 1% is found down to 600 km depth beneath a portion of the Pacific–Antarctic Ridge (PAR) close to the Balleny Islands (BI). The AS–MBL, PAR and RS anomalies are remarkable because they are continuous from the asthenosphere down to transition zone depths, and they are not likely to be artefacts of the method, as shown by synthetic experiments in Section 5. Moreover, even when

setting the limit of significance at a more severe level of two standard deviations (contour at −1.6% on Fig. 7), they still extend down to 400 km depth at least. Although the Crozet–Kerguelen and the Southeast Pacific Ocean anomalies also display a strong contrast at 200–300 km (> 3%), they do not present such characteristics.

For understanding the significance of these deeply rooted low-velocity anomalies, a comparison with the results of Ritsema and van Heijst [12] can be helpful. Our tomographic approach is close to the work of these authors in the sense that they analyzed a global data set of fundamental and higher mode Rayleigh waves. In addition to surface waves, they also used body waves and normal mode splitting to constrain the structure down to the lower mantle. In the upper mantle part of their global model S20RTS [12], the Amundsen Sea, the Ross Sea region and the Pacific–Antarctic Ridge in the vicinity of the Balleny Islands are underlain by a large, negative anomaly down to 300 km depth only. The anomaly does not stretch to Marie Byrd Land. The lateral resolution of S20RTS is no better than 2000 km, while in our regional study, the lateral resolution is estimated to a few hundred kilometers (see Section 5). Our three deep, vertical low-velocity anomalies (labelled AS–MBL, RS and PAR) present a width of about 700–800 km below 300 km depth. This could explain why these deep features are not imaged in S20RTS. The shallow, large, negative anomaly of this area in S20RTS is however connected to a structure sinking down to 700 km depth southeast of New Zealand. As it is situated on the edge of our regional model we cannot make sure whether it corresponds to our anomaly labelled PAR or if it is an independent structure.

We will now focus on the three remarkable deep vertical anomalies, observed in Fig. 7. In the following section, we investigate in details the robustness of these structures.

5. Synthetic experiments

The first synthetic experiment is designed to evaluate the degree of vertical smearing likely to affect the shallow parts of our tomographic model. The idea is to check whether the observed variations in the maximum depth of the shallow low-velocity layer could be attributed to lateral variations in the vertical resolution that would result in different amount of vertical smearing. In other words, regions where the retrieved shallow low-velocity layer is thin would be better constrained than regions where it seems to be more deeply rooted. We have performed a full synthetic experiment following the procedure described in [18]. The 'full' synthetic test reproduces both steps of our tomographic approach. For each path of the actual coverage, we first compute a synthetic seismogram in the input velocity model. We then use our automated waveform inversion to invert each synthetic waveform for a path average SV velocity model before combining these 1D velocity models in a tomographic inversion to retrieve the local structure. The synthetic inversion is performed using the same number of overtones and the same a priori values as the actual inversion. The input velocity model is our smoothed PREM model in which we have added a −10% velocity perturbation from the Moho down to 125 km depth (Fig. 8a). The retrieved structure is smoother than the input structure (Fig. 8b), but vertical smearing is weak with no strong lateral variation. Keeping in mind that some of the observed broad, downward extensions of the low-velocity layer in Fig. 7 display velocity contrasts reaching 3% below 200 km and extending down to 600 km depth with an amplitude greater than 1%, it is very unlikely from the synthetic test of Fig. 8 that they result from vertical smearing of shallow structures. Moreover, this test shows that the tomographic method has a tendency to produce spurious anomalies below 175 km depth. The amplitude of these anomalies reaches 1.1% in Fig. 8b. However, since the spurious anomalies are opposite in sign to the shallow input perturbation, the observed negative anomalies (Fig. 7) which extend continuously down to transition zone depths without any change of sign are not likely to be an artefact. On the other hand, the negative anomalies (1–2%) found beneath the high-velocity lid (> 10%) of East Antarctica may suffer from this artefact and are thus not robust.

We have then conducted a second synthetic experiment to evaluate our ability to resolve a low-velocity anomaly located below the asthenosphere. Our input velocity model is now the same smoothed version of PREM in which we have added a −5% SV-wave velocity anomaly centered in the Ross Sea at 75°S and 179°W (Fig. 9a), a region where we found the deepest low-velocity structures. The anomaly is located between 250 and 350 km depth and is elongated in the east–west direction, with a lateral extension of about 700 km × 1000 km. The synthetic experiment is again a 'full' test conducted as in Debayle et al. [18]. The output model is shown in Fig. 9b. Horizontal smearing is observed along the dominant direction of paths. However, vertical smearing is small and the input anomaly, although smoothed by the tomographic inversion, is retrieved at the right location and right depth. This confirms that our fundamental mode and overtones data set allows us to isolate a deep low-velocity anomaly from the shallower and the deeper structure and to recover its geometry and location, even though its amplitude is underestimated. This latter point suggests that the actual velocity contrast of the structures could be underestimated in the inverted model. We have tested whether such a deep structure could be resolved without the overtone information. For this purpose we have performed a new 'full' synthetic experiment in which we tried to retrieve the same model as in Fig. 9a but without the help of the overtones. The result of the synthetic experiment is shown in Fig. 9c and confirms that without overtones, it is neither possible to locate properly in depth the input anomaly nor to recover its amplitude and shape. An anomaly is picked up by the fundamental mode, but due to its poor sensitivity at depths greater than 250 km in our period range of analysis (50–160 s), it is weaker than expected and shifted towards shallow depths, where the fundamental mode has the largest sensitivity. This underlines the importance of the higher mode data to study deep structures.

From this series of 'full' synthetic tests it seems difficult to invoke artefacts brought by the tomographic method to explain the deeply rooted low-velocity anomalies observed beneath the coast of

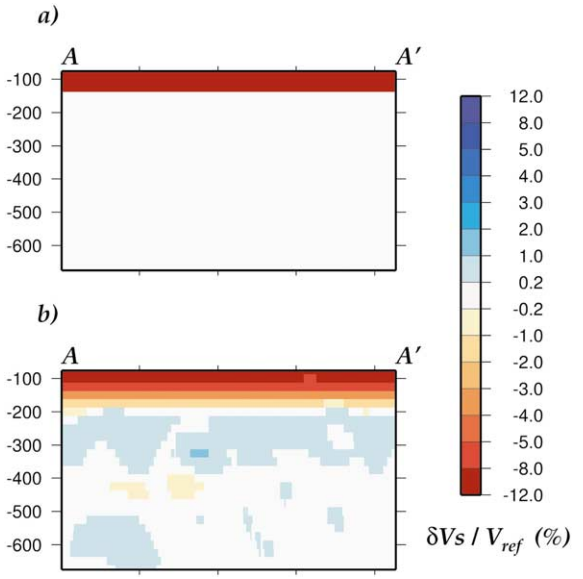

Fig. 8. Synthetic experiment to test the vertical smearing of a uniform shallow structure. (a) Input model and (b) output model. The input SV velocity perturbation of −10% extends from Moho down to 125 km depth beneath the whole region under study. The cross-section is along the AA′ profile (Fig. 7a). Note that the spurious velocity anomalies deeper than 175 km are smaller than 1.1%.

Marie Byrd Land, the Pacific–Antarctic Ridge and the Ross Sea region (cross-sections BB′, CC′ and DD′ in Fig. 7), even though these experiments did not test all the effects that could impair the results. As it has been discussed in detail in [18], the approximations used in the theory are likely to be valid in our frequency band of analysis for relatively short paths and errors on the a priori crustal structure should not affect the model for depths greater than 200 km, largely constrained by long-period higher modes less sensitive to the shallow structure.

If the vertical deep low-velocity anomalies we image are real, it is tempting to associate them with upwelling of hot and less viscous material. However, their lateral extent is larger than the proposed width for a mantle plume tail at these depths [35]. We have therefore performed a synthetic experiment to investigate in more detail the degree of horizontal smearing in our tomographic inversion. For this purpose, we only need to test the final tomographic procedure. For a realistic experiment, the input model is 3SMAC in which

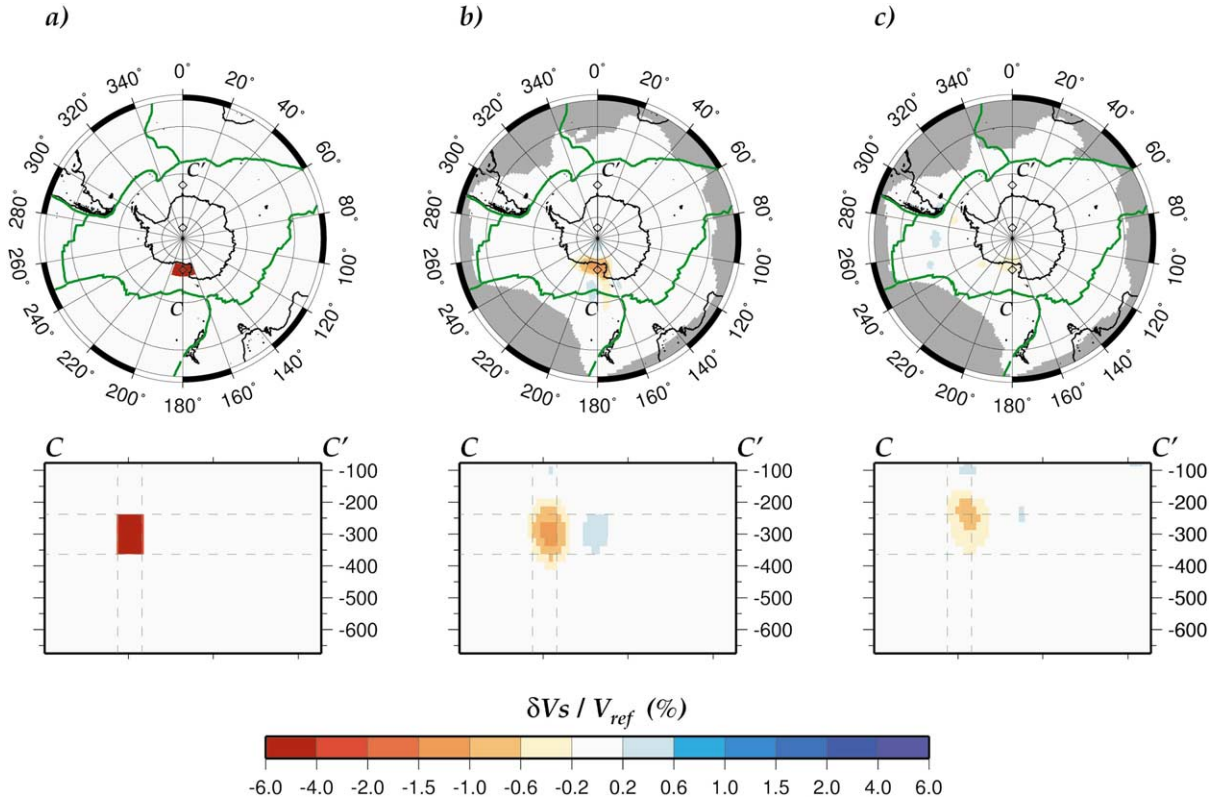

Fig. 9. Synthetic experiment to test the ability to retrieve a velocity perturbation below the asthenosphere with and without the use of overtones. (a) Input model, (b) output model with the overtones and (c) output model with the fundamental mode only. Top maps are the model at 300 km depth and the bottom cross-sections are along profile CC′ (Fig. 7c). We try to retrieve a 700 km×1000 km wide SV velocity perturbation of −5% located between 250 and 350 km depth. Gray dashed lines mark the depth and lateral limits of the input perturbation. Note that the spurious positive anomalies are smaller than 0.6%.

the low-velocity perturbations modelling the hotspots of Duncan and Richards's [36] distribution have been reinforced. The 3SMAC model actually uses Duncan and Richards's [36] distribution with several additional 'new' hotspots [25]. The perturbations are about 200 km wide and 5% slower than the embedding structure (Fig. 10a). All the hotspots located in the central part of the model (i.e. where the a posteriori error is smaller than 0.04 km/s) have been retrieved even though they have been smoothed by the tomographic process. We present in Fig. 10b the results for the two hotspots of the Ross Sea region (Erebus and Balleny), as the deep velocity anomalies of the inverted model that we focus on are found in this region. The output anomalies in Fig. 10b only suffer a slight shift compared to the location of the input perturbations (towards the north for Balleny and towards the southeast for Erebus). Their amplitude is attenuated and they have a lateral extension of about 800–1000 km. A similar experiment shows that a 100 km wide anomaly with a 8% perturbation produces about the same pattern through the tomographic method. This suggests that the width of the deep velocity anomalies observed in cross-sections BB′, CC′ and DD′ (Fig. 7) can be reconciled with a plume conduit narrower than 200 km but with a stronger velocity contrast.

6. Discussion

The hypothesis of a large plume (∼3000 km

wide in the asthenosphere) located beneath the West Antarctic Rift and including Marie Byrd Land and the Ross Sea region, has recently been discussed (e.g. [5,7,9]. It is supported by the similarity of large amount of subglacial volcanic rocks and by the chemistry of the sparse exposed volcanic rocks. For example, Marie Byrd Land is a volcanic province whose basalts are indistinguishable from those on oceanic islands [8]. Like other basalts found in the West Antarctic Rift, they have erupted in the last 30 Ma [4] and are difficult to reconcile with a shallow source related to the rifting, as the main period of extension in the West Antarctic Rift occurred in the late Mesozoic [5,9]. The presence of a topographic dome centered in the province, whose growth is closely linked to the volcanism [8], also favors the presence of a plume beneath the region. In the Balleny Islands, the chemistry of the volcanic rocks also suggests a deep-seated plume origin [7].

Our final SV-wave velocity model presents two vertical low-velocity structures extending continuously down to transition zone depths beneath the Amundsen Sea–Marie Byrd Land and beneath the Pacific–Antarctic Ridge near the Balleny Islands (MBL and PAR in Fig. 7b, c and d). The low-velocity anomaly of the Ross Sea (RS in Fig. 7c) could be considered as a third one, though its amplitude is close to the a posteriori error between 250 and 400 km depth (Fig. 7g) so that vertical connection between the anomalies shallower than 250 km and deeper than 400 km remains uncertain. Regarding the local geology, the plume hypothesis seems to be a good candidate to explain these deep anomalies. Following this idea we now discuss the implication of such plume prints in terms of upwelling material beneath the region.

Assuming that they are related in some way to the volcanism of the region above them, close links between the three structures are suggested by the very similar geochemical characteristics of the Cenozoic volcanic rocks present in Marie Byrd Land, the Balleny Islands and the Ross Sea region [4,7]. Recent laboratory experiments suggest that, in a chemically heterogeneous mantle, it is possible to generate upwelling that would take the form of broad domes [37]. Connections

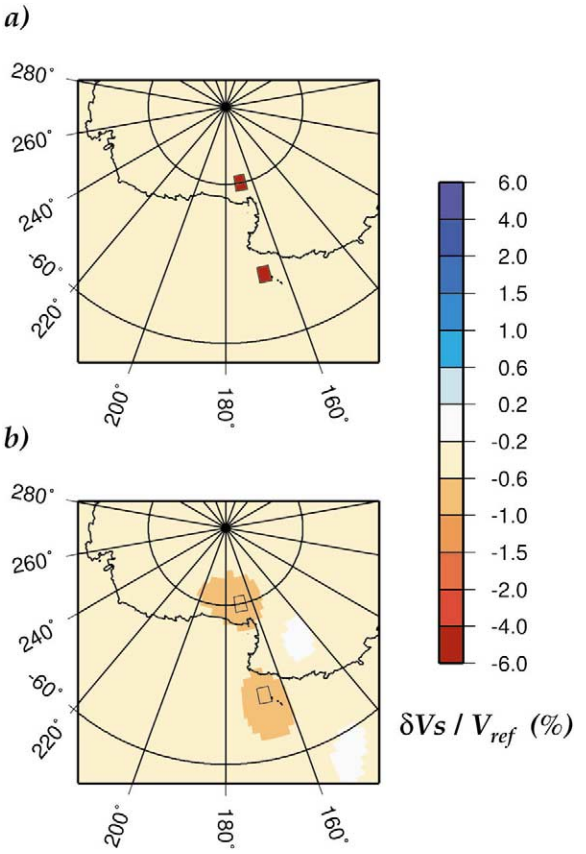

Fig. 10. Synthetic experiment to test the lateral resolution of the tomographic inversion. (a) Input model and (b) output model. The input model is 3SMAC at 200 km depth in which the perturbations related to the hotspots of Duncan and Richards's [36] distribution have been reinforced (−5% SV velocity perturbations, 200 km wide). We present a zoom on the Ross Sea region hotspots, Erebus (south) and Balleny (north). Black boxes mark the position of the input perturbations. Note that on this kind of map, the north is to the bottom of the picture.

between the structures of the Balleny Islands and the Ross Sea may be inferred from cross-section CC′ (Fig. 7c) at least at depths shallower than 200 km. At greater depths a broad low-velocity region with amplitude smaller than 1% encompasses the two vertical structures. However error maps suggest that at depths larger than 300 km, only seismic anomalies with an amplitude larger than 1% are well resolved (Fig. 7f, g and h) and synthetic tests (Fig. 10) demonstrate that these significant anomalies can be reconciled with two narrow

plume tails, well separated laterally. Moreover, in view of the lateral resolution, the structure beneath Marie Byrd Land is very unlikely to be connected to the Ross Sea and Balleny Islands structures at depth as the deep velocity anomaly retrieved beneath Marie Byrd Land is clearly separated from the other two anomalies. Our results therefore advocate the existence of two, maybe three, distinct mantle plumes underlying or in the close vicinity of Marie Byrd Land, the Balleny Islands and the Ross Sea region, instead of a single large one.

At depth greater than 300 km, the deep vertical low-velocity anomaly on cross-sections CC′ and DD′ (Fig. 7c and d) is located beneath the Pacific–Antarctic Ridge and is shifted by 700 km from the surface location of the closest hotspot, the Balleny Islands. Keeping in mind that the lateral resolution is of the order of few hundred kilometers, it is possible to suggest a connection between the deep anomaly and this hotspot. An explanation for the shift between the supposed mantle upwelling and the hotspot surface expression could be the migration of plume material beneath the lithosphere. Such an explanation may be supported by cross-section DD′ in Fig. 7.

Anderson et al. [38] suggested that the asthenosphere is neither homogeneous nor isothermal. They used the fundamental mode global surface wave model of Zhang and Tanimoto [11] which presents a lateral resolution of about 1000 km in the uppermost 200 km of the mantle to suggest that the upper mantle is characterized by vast domains of high temperature rather than small regions surrounding hotspots. Our more detailed regional model agrees with the idea of several large, low-velocity domains surrounding hotspots in the oceanic asthenosphere rather than small, low-velocity regions. We observe that there is no systematic link between low-velocity anomaly and hotspot. For example, the Kerguelen hotspot is located in a well constrained region where the fundamental mode coverage is good and is not underlain by low velocities in the uppermost 200 km. We also note that the broad, low-velocity anomalies in the Southeast Pacific Ocean (SEP in Fig. 7a) and in the south of Kerguelen plateau (Fig. 4c) are not related to current oceanic ridges in the uppermost 200 km of the mantle and are difficult to associate with any hotspot at the surface. Anderson et al. [38] suggested that some of the low velocities observed in the asthenosphere could reflect previous positions of migrating ridges. This kind of model seems difficult to reconcile with the anomalies in the Southeast Pacific Ocean and the South Indian Ocean since they persist at relatively large depths in the mantle. Further interpretations of these asthenospheric structures would require an improved knowledge of both the geology and past plate motion in the region.

Anderson et al. [38] did not find evidence for deep thermal perturbation beneath the hotspots. We suggest that this is likely to be due to the decrease in sensitivity of their fundamental mode data set at depths larger than 200 km. Our results show that a deep source may exist beneath at least some of the hotspots in Antarctica. This imaging of deep low-velocity structures connected to large regions of low seismic velocities in the asthenosphere could be in partial agreement with the model of Phipps Morgan et al. [39]. They proposed that the oceanic asthenosphere is fed by plumes from the lower mantle and is a region of large lateral flows from the 'feeding conduits' towards the ridges. Our tomographic model does not allow to discuss whether the deep vertical low-velocity structures that we observe in the upper mantle extend in the lower mantle, but the cross-sections in Fig. 7 is an argument for strong lateral flows in the asthenosphere connecting the deep vertical structures to the ridges (cross-section BB′) or to some of the reported hotspots near the surface (cross-section CC′).

Further discussion on these deep low-velocity structures and their potential role in mantle dynamics needs a more detailed imaging at greater depths. The lateral resolution must be enhanced to better constrain the geometry of these deep low-velocity structures and to confront their seismic signature with laboratory experiments and numerical simulations of mantle plumes. Phipps Morgan et al. [39] situate the source of the feeding plumes in the lower mantle. Images at greater depths would allow to know whether these structures are really originating from below the tran-

sition zone as suggested by model S20RTS [12] which detects low-velocities beneath the Pacific–Antarctic Ridge close to the Balleny Islands, the Ross Sea region and off Marie Byrd Land in the depth range 800–1000 km. Teleseismic body waves often provide complementary information to surface wave studies. High-resolution body wave tomographies require a dense seismic coverage which is not available at high southern latitudes yet. Our knowledge of the upper mantle beneath the Antarctic plate is therefore likely to continue to rely mainly on surface wave analysis in the near future. Antarctica is thus a region where it is strongly needed to improve the surface wave tomography techniques for example by using seismic wave propagation theories more accurate than the classical geometrical theory as it has been explored in many recent works.

Acknowledgements

This work is supported by the INSU program 'Intérieur de la Terre'. Supercomputer facilities were provided by the French 'Institut for Development and Resources in Intensive Scientific Computing' (IDRIS). The maps and the cross-sections presented in this paper have been made using the GMT software [40]. We thank reviewers Anne Davaille, Ban-Yuan Kuo and Jeroen Ritsema for their helpful and constructive comments.*[VC]*

References

[1] I.W.D. Dalziel, D.H. Elliot, West Antarctica: problem child of Gondwanaland, Tectonics 1 (1982) 3–19.
[2] G. Roult, D. Rouland, Antarctica I: Deep structure investigations inferred from seismology; a review, Phys. Earth Planet. Inter. 84 (1994) 15–32.
[3] S.C. Cande, J.M. Stock, R.D. Müller, T. Ishihara, Cenozoic motion between East and West Antarctica, Nature 404 (2000) 145–150.
[4] G. Wörner, Lithospheric dynamics and mantle sources of alkaline magmatism of the Cenozoic West Antarctic Rift System, Glob. Plan. Chan. 23 (1999) 61–77.
[5] J.C. Behrendt, W.E. LeMasurier, A.K. Cooper, F. Tessensohn, A. Tréhu, D. Damaske, Geophysical studies of the West Antarctic Rift System, Tectonics 10 (1991) 1257–1273.
[6] M.H. Ritzwoller, N.M. Shapiro, A.L. Levshin, G.M. Leahy, Crustal and upper mantle structure beneath Antarctica and surrounding oceans, J. Geophys. Res. 106 (2001) 30645–30670.
[7] S.R. Hart, J. Blusztajn, W.E. LeMasurier, D.C. Rex, Hobbs Coast Cenozoic volcanism: Implication for the West Antarctic rift system, Chem. Geol. 139 (1997) 223–248.
[8] W.E. LeMasurier, C.A. Landis, Mantle-plume activity recorded by low-relief erosion surfaces in West Antarctica and New Zealand, GSA Bull. 108 (1996) 1450–1466.
[9] J.C. Behrendt, W.E. LeMasurier, A.K. Cooper, The West Antarctic Rift System – A propagating rift 'captured' by a mantle plume?, in: Y. Yoshida, K. Kaminuma, K. Shiraishi (Eds.), Recent Progress in Antarctic Earth Science, Terra Sci., Tokyo, 1992, pp. 315–322.
[10] B.C. Storey, The role of mantle plumes in continental breakup: case histories from Gondwanaland, Nature 377 (1995) 301–308.
[11] Y.-S. Zhang, T. Tanimoto, High-resolution global upper mantle structure and plate tectonics, J. Geophys. Res. 98 (1993) 9793–9823.
[12] J. Ritsema, H.J. van Heijst, Seismic imaging of structural heterogeneity in Earth's mantle: Evidence for large-scale mantle flow, Sci. Prog. 83 (2000) 243–259.
[13] G. Roult, D. Rouland, J.P. Montagner, Antarctica II: Upper-mantle structure from velocities and anisotropy, Phys. Earth Planet. Inter. 84 (1994) 33–57.
[14] S. Danesi, A. Morelli, Group velocity of Rayleigh waves in the Antarctic region, Phys. Earth Planet. Inter. 122 (2000) 55–66.
[15] S. Danesi, A. Morelli, Structure of the upper mantle under the Antarctic Plate from surface wave tomography, Geophys. Res. Lett. 28 (2001) 4395–4398.
[16] E. Debayle, SV-wave azimuthal anisotropy in the Australian upper-mantle: preliminary results from automated Rayleigh waveform inversion, Geophys. J. Int. 137 (1999) 747–754.
[17] M. Cara, J.J. Lévêque, Waveform inversion using secondary observables, Geophys. Res. Lett. 14 (1987) 1046–1049.
[18] E. Debayle, J.J. Lévêque, M. Cara, Seismic evidence for a deeply rooted low-velocity anomaly in the upper mantle beneath the northeastern Afro/Arabian continent, Earth Planet. Sci. Lett. 193 (2001) 423–436.
[19] E. Debayle, J.J. Lévêque, Upper mantle heterogeneities in the Indian Ocean from waveform inversion, Geophys. Res. Lett. 24 (1997) 245–248.
[20] E. Debayle, B.L.N. Kennett, The Australian continental upper mantle: Structure and deformation inferred from surface waves, J. Geophys. Res. 105 (2000) 25423–25450.
[21] K. Priestley, E. Debayle, Seismic evidence for a moderately thick lithosphere beneath the Siberian Platform, Geophys. Res. Lett. 30 (2003) 1118, 10.1029/2002GL015931.
[22] S. Pilidou, O. Gudmundsson, E. Debayle, K. Priestley,

Upper mantle SV-wavespeed heterogeneity beneath the north Atlantic, EOS Trans. Am. Geophys. Union 83 (47) (2002), Fall Meet. Suppl. F1040.
[23] J.J. Lévêque, M. Cara, D. Rouland, Waveform inversion of surface wave data: test of a new tool for systematic investigation of upper mantle structures, Geophys. J. Int. 104 (1991) 565–581.
[24] A.M. Dziewonski, D.L. Anderson, Preliminary reference Earth model, Earth Planet. Inter. 25 (1981) 297–356.
[25] H.C. Nataf, Y. Ricard, 3SMAC: an a priori tomographic model of the upper mantle based on geophysical modeling, Phys. Earth Planet. Inter. 95 (1995) 101–122.
[26] J.P. Montagner, Regional three-dimensional structures using long-period surface waves, Ann. Geophys. 4 (1986) 283–294.
[27] C.E. Nishimura, D.W. Forsyth, The anisotropic structure of the upper mantle in the Pacific, Geophys. J. 96 (1989) 203–229.
[28] J.J. Lévêque, E. Debayle, V. Maupin, Anisotropy in the Indian Ocean upper mantle from Rayleigh- and Love-waveform inversion, Geophys. J. Int. 133 (1998) 529–540.
[29] J. Ritsema, H.J. van Heijst, J.H. Woodhouse, Complex shear wave velocity structure imaged beneath Africa and Iceland, Science 286 (1999) 1925–1928.
[30] D.W. Forsyth, R.L. Ehrenbard, S. Chapin, Anomalous upper mantle beneath the Australian–Antarctic Discordance, Earth Planet. Sci. Lett. 84 (1987) 471–478.
[31] B.-Y. Kuo, C.-H. Chen, Y.-S. Zhang, A fast velocity anomaly to the west of the Australian–Antarctic Discordance, Geophys. Res. Lett. 23 (1996) 2239–2242.
[32] R.D. Müller, W.R. Roest, J.-Y. Royer, L.M. Gahagan, J.G. Scalter, Digital isochrons of the world's ocean floor, J. Geophys. Res. 102 (1997) 3211–3214.
[33] N.M. Shapiro, M.H. Ritzwoller, Monte-Carlo inversion for a global shear-velocity model of the crust and upper mantle, Geophys. J. Int. 151 (2002) 88–105.
[34] B.L.N. Kennett, E.R. Engdhal, R. Buland, Constraints on seismic velocities in the Earth from traveltimes, Geophys. J. Int. 122 (1995) 108–124.
[35] R.W. Griffiths, I.H. Campbell, Stirring and structure in mantle starting plume, Earth Planet. Sci. Lett. 99 (1990) 66–78.
[36] R.A. Duncan, M.A. Richards, Hotspots, mantle plumes, flood basalts, and true polar wander, Rev. Geophys. 29 (1991) 31–50.
[37] A. Davaille, Simultaneous generation of hotspots and superswells by convection in a heterogeneous planetary mantle, Nature 402 (1999) 756–760.
[38] D.L. Anderson, T. Tanimoto, Y.-S. Zhang, Plate tectonics and hotspots: The third dimension, Science 256 (1992) 1645–1651.
[39] J. Phipps Morgan, W.J. Morgan, Y.-S. Zhang, W.H.F. Smith, Observational hints for a plume-fed, suboceanic asthenosphere and its role in mantle convection, J. Geophys. Res. 100 (1995) 12753–12767.
[40] P. Wessel, W.H.F. Smith, New version of the Generic Mapping Tools released, EOS Trans. Am. Geophys. Union 76 (1995) 329.